12

Electro-Hydrodynamics of Micro-Discharges in Gases at Atmospheric Pressure

O. Eichwald, M. Yousfi, O. Ducasse, N. Merbahi,
J. P. Sarrette, M. Meziane and M. Benhenni
University of Toulouse, University Paul Sabatier,
LAPLACE Laboratory,
France

1. Introduction

Micro-discharges are specific cold filamentary plasma that are generated at atmospheric pressure between electrodes stressed by high voltage. As cold plasma or non-thermal plasma, we suggest that the energy of electrons inside the conductive plasma is much higher than the energy of the heaviest particles (molecules and ions). In such kind of plasma, the temperature of the gas remains cold (i.e. more or less equal to the ambient temperature) unlike in the field of thermal plasmas where the gas temperature can reach some thousands of Kelvin. This high level of temperature can be measured for example in plasma torch or in lightning.
The conductive channels of micro-discharges are very thin. Their diameters are estimated around some tens of micrometers. This specificity explains their name: micro-discharge. Another of their characteristic is their very fast development. In fact, micro-discharges propagate at velocity that can attain some tens of millimetres per nanosecond i.e. some 10^7 $cm.s^{-1}$. This very fast velocity is due to the propagation of space charge dominated streamer heads. The space charge inside the streamer head creates a very high electric field in which the electrons are accelerated like in an electron gun. These electrons interact with the gas and create mainly ions and radicals. In fact, the energy distribution of electrons inside streamer heads favours the chemical electron-molecule reactions rather than the elastic electron-molecule collisions. Therefore, micro-discharges are mainly used in order to activate chemical reactions either in the gas volume or on a surface (Penetrante & Schultheis, 1993, Urashima &Chang, 2010, Foest et al. 2005, Clement, 2001).
Several designs of plasma reactors are able to generate micro-discharges. The most convenient and the well known is probably the corona discharge reactor (Loeb, 1961&1965, Winands, 2006, Ono & Oda a, 2004, van Veldhuizen & Rutgers, 2002, Briels et al., 2006). Corona micro-discharges reactor has at least two asymmetric electrodes i.e. with one of them presenting a low curvature that introduces a pin effect where the geometric electric field is enhanced. The corona micro-discharges are initiated from this high geometric field area. Some samples of corona reactor geometries are shown in Fig. 1.
The transient character and the small dimensions make some micro-discharges parameters, like charged and radical densities, electron energy or electric field strength, difficult to be accessible to measurements. Therefore, the complete simulation of the discharge reactor, in complement to experimental study can lead to a better understanding of the physico-

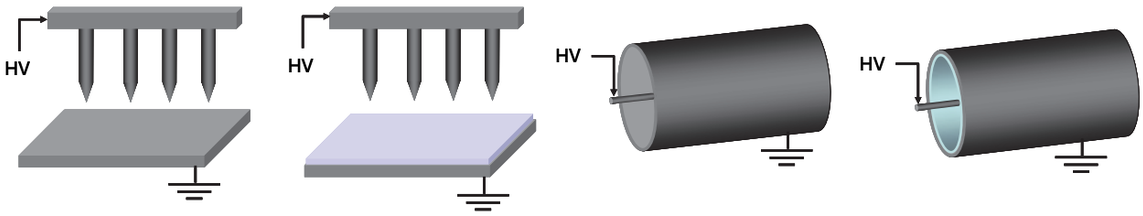

Fig. 1. Sample of pin-to-plane and wire-to-cylinder corona discharge reactors. The light blue material corresponds to a dielectric material. Depending on applications, design and reactor efficiency, the High Voltage (HV) shape can be DC, pulsed, AC or a combination of them.

chemical activity triggered by the micro-discharge during the plasma process. All these information can be used in order to improve the reactor design and to achieve the best operating conditions (such as the reactor geometry, the flue gas resident time, the applied voltage shape and magnitude, among others) as a function of the chosen applications.

The present chapter is devoted to description of the main electro-hydrodynamics phenomena that take place in non-thermal plasma reactors at atmospheric pressure activated by corona micro-discharges. The first section describes the micro-discharges characteristics using the experimental results obtained in a mono pin-to-plane reactor stressed by either DC or pulsed high voltage. The physics of the micro-discharges development is explained and a complete hydrodynamics model is proposed based on the moments of Boltzmann equations for charged and neutral particles. Then before to conclude, the previous described model is used in order to simulate the strongly coupled chemical and hydrodynamics phenomena generated by micro-discharges in a non thermal plasma reactor.

2. Description of positive corona micro-discharges

2.1 Introduction

In this first section, we describe the main characteristics of the corona micro-discharge formation and development as a function of several operating parameters such as the geometry of electrodes or the shape and magnitude of applied high voltage. Then, based on Boltzmann kinetic theory, we describe the strongly coupled electrical, hydrodynamics and chemical phenomena that take place in a compressible gas crossed by micro-discharges.

2.2 Positive corona micro-discharge under DC voltage condition

Let consider a mono pin-to-plane electrode corona reactor filled with dry air at atmospheric pressure and ambient temperature (Dubois et al., 2007). A DC high voltage supply is connected to the pin through a mega ohm resistor. When the applied voltage is raised gradually there is no sustained discharge current as much as the electrical gap field remains less than the onset one. Then, a sudden current pulse appears marking the beginning of the self sustained onset streamer regime. The associated current pulses occur intermittently and randomly and the mean current is very low (of few μA). Using a CCD camera with a large time shutter, we can observe a low intensity spot light just around the pin (see Fig. 2a). If we continue to increase the DC voltage, the current pulses vanish. However, the spot light near the point is always observed but with a quite higher intensity (see Fig. 2b). This regime corresponds to the classical glow corona discharge which is characterised by a drift of charged particles in the inter-electrode gap. The average current can reach some tens of μA.

For a high voltage threshold value, some regular repetitive current pulses appear with a repetition frequency of some tens of kHz and a magnitude of some tens to hundred of mA. Each current pulse lasts some hundred of nanoseconds and corresponds to the propagation of a mono-filament corona micro-discharge shown in Fig. 2c.

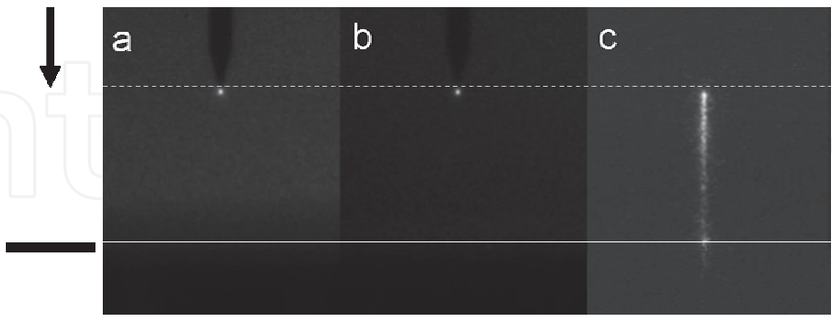

Fig. 2. Photography of the different corona discharge regimes under positive DC voltage condition (inter-electrode distance = 7mm, pin radius = 20 µm, dry air, atmospheric pressure). a: onset streamer, DC voltage magnitude = 3.2kV, time camera shutter = 1s, b: glow discharge, DC voltage magnitude = 5kV, time camera shutter = 10ms, c: streamer micro-discharge, DC voltage magnitude = 7.2kV, time camera shutter = 10µs (Eichwald et al., 2008).

More detailed information on the spatio-temporal evolution of the micro-discharge can be obtained thanks to the analysis of the streak camera picture shown in Fig. 3 and the corresponding current pulse shown in Fig. 4 (Eichwald et al., 2008, Marode, 1975). In Fig. 3, the X-axis is the time axis while the Y-axis is the inter-electrode distance. The electrode location is shown in the drawing at the left side of Fig. 3. For a given time on the X-axis, the light emission of the micro-discharge filament at each position is focused along the corresponding Y-axis coordinate. When 8.2kV is applied to the pin, three main phases can be distinguished in the corona micro-discharge development. The first one corresponds to the primary streamer propagation from the anode pin towards the cathode plane. The primary streamer propagates a luminous spot (called streamer head) which leaves the first narrow luminous trail shown on the streak picture of Fig. 3. During this first phase, the current rapidly increases as shown in Fig. 4 between 50ns and 75ns. The second phase

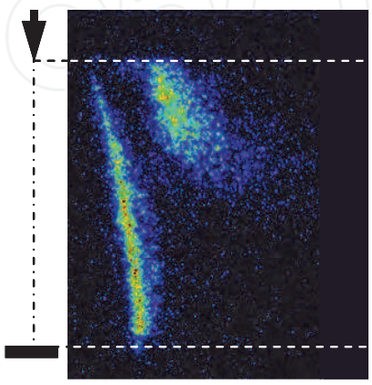

Fig. 3. Streak camera picture of a corona micro-discharge: Inter-electrode distance = 7mm, pin radius = 20 µm, dry air, atmospheric pressure, DC voltage magnitude = 8.2kV

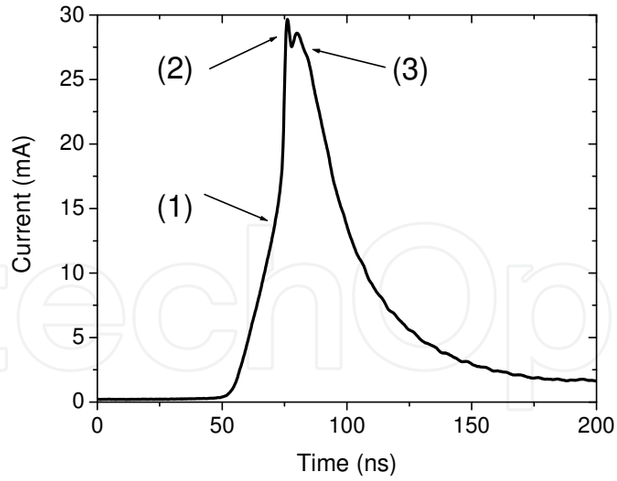

Fig. 4. Instantaneous micro-discharge current (inter-electrode distance = 7mm, pin radius = 20 μm, dry air, atmospheric pressure, DC voltage magnitude = 8.2kV)

corresponds to the arrival of the primary streamer at the cathode. It is associated to both the sudden increase of the current pulse at around 75ns (see Fig. 4) and the first current peak. In the present experimental conditions, the current pulse magnitude reaches a maximum of 30mA. On the current curve of Fig. 4, we also observe that the primary streamer needs about 25ns to cross the inter electrode gap and to reach the cathode plane 7mm underneath the pin. Thereby, the mean primary streamer velocity can be estimated of about 3×10^{7}cm s^{-1}. We also observe in Fig. 3 the development of a secondary streamer (Sigmond, 1984) starting from the point when the primary streamer arrives at the cathode plane. The associated light emission is more diffuse on the streak picture because the radiative species are distributed along the pre-ionized channel. The development and propagation of the secondary streamer induce a second current peak (see Fig. 4). Finally, each current pulse is characterised by the propagation of primary and secondary streamers which in turn create the thin ionized channels of the micro-discharge shown in Fig. 2c.

2.3 Positive corona micro-discharge under pulsed voltage condition

The morphology of micro-discharges under pulse voltage condition is quite different from the case of DC voltage condition (van Veldhuizen & Rutgers, 2002, Abahazem et al. 2008). However, we will see at the end of the present section the correspondence between both regimes using a large voltage pulse width. Fig. 5 shows a sample of a high voltage pulse applied on the pin of a pin-to-plane corona reactor and the resulting measured current pulse. The pulse voltage width is first chosen in order to obtain only one micro-discharge per pulse. The experimental conditions are very similar to those used for the DC voltage study described in previous section 2.2. In Fig. 5, the two current peaks superposed with the increasing and decreasing fronts of the pulse voltage are two capacitive current pulses generated by the equivalent capacitance of the pin-to-plane electrode configuration. The micro-discharge current pulse is positioned at time t=0ns in Fig. 5. A detailed description of this peculiar current pulse can be seen in Fig. 6. A rapid comparison with the DC current pulse in Fig. 4 indicates that the current pulse magnitude under pulse voltage condition is much higher (~175mA) than in the DC voltage case (~30mA). In fact, the ICCD time

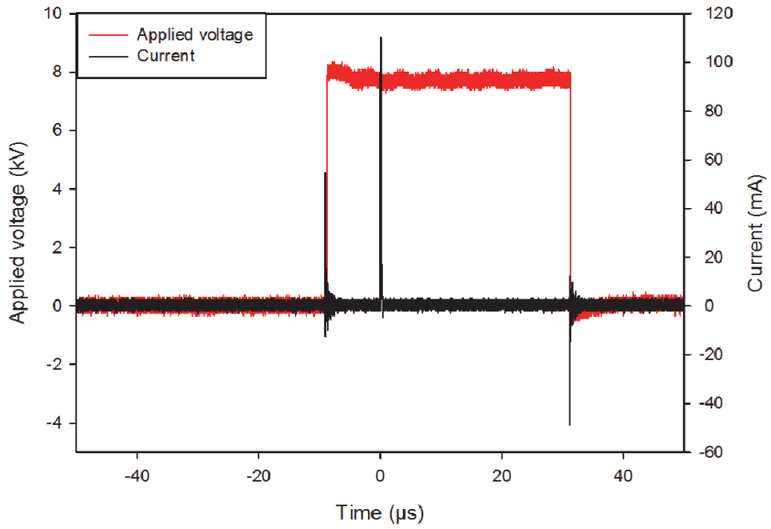

Fig. 5. Instantaneous measured current for pulsed voltage conditions: Maximum voltage magnitude=8kV, pulse voltage width=40μs, inter-electrode distance=8mm, pin radius=25μm, dry air at atmospheric pressure.

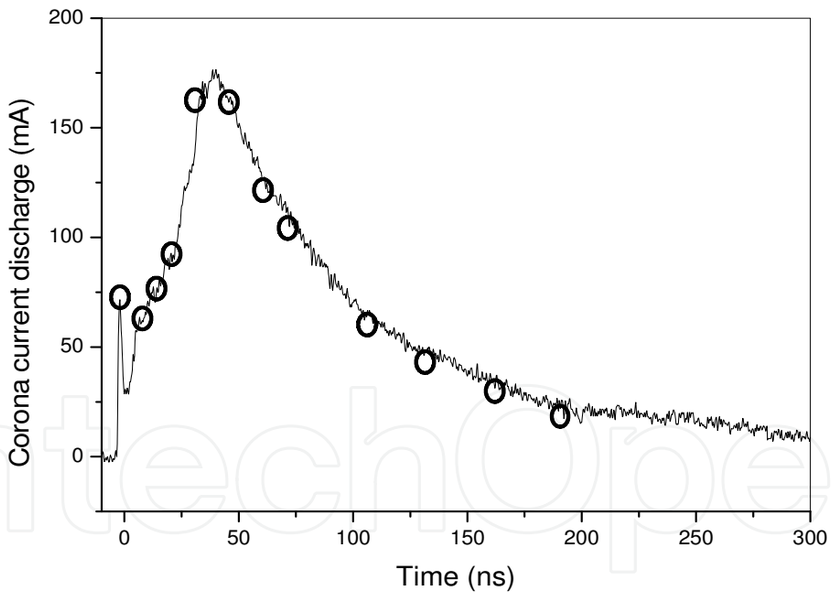

Fig. 6. Instantaneous corona current for pulsed voltage conditions: Maximum voltage magnitude=8kV, pulse voltage width=40μs, inter-electrode distance=8mm, pin radius=25μm, dry air at atmospheric pressure.

integrated picture of Fig. 7 clearly shows that there are several streamers starting from the pin towards the plane. This branching mechanism occurs in pulsed voltage conditions and therefore gives a higher discharge current than in the case of DC voltage.

The evolution of the corona current in Fig. 6 is characterized by a first peak of about 70mA with a short duration (around 4ns) corresponding to the discharge ignition due to the

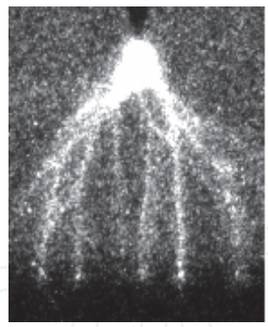

Fig. 7. Time integrated picture of corona discharge in dry air at atmospheric pressure for a time exposure of 10ms: Maximum voltage magnitude=8kV, pulse voltage width=40µs, inter-electrode distance=8mm and pin radius=25µm.

intense ionization processes generated by the high geometric electric field near the pin. This phenomenon can be seen in the first picture of Fig. 8 which shows an intensive spot light around the pin. After this first current peak, as soon as the electron avalanches reach a critical size, the accumulated charge space splits into several streamer heads that begin to propagate towards the cathode (see Fig. 8). During this primary streamer propagation, the corona current begins to steeply increase up to reach a peak value of about 175mA at the streamers arrival at the cathode for a time around 50ns (see Fig. 6). The streamer branches arrive separately at the cathode with an average propagation velocity of about 2.7×10^7 cm.s^{-1}. Above this instant, the corona current peak, after a first decrease due to transition between displacement and conduction currents, slows down during a short duration (around 70ns) corresponding to the secondary streamer propagation. This is then followed by a slower and monotonic fall of the corona current corresponding to the relaxation time that lasts above the 300ns displayed in the time axis of Fig. 6.

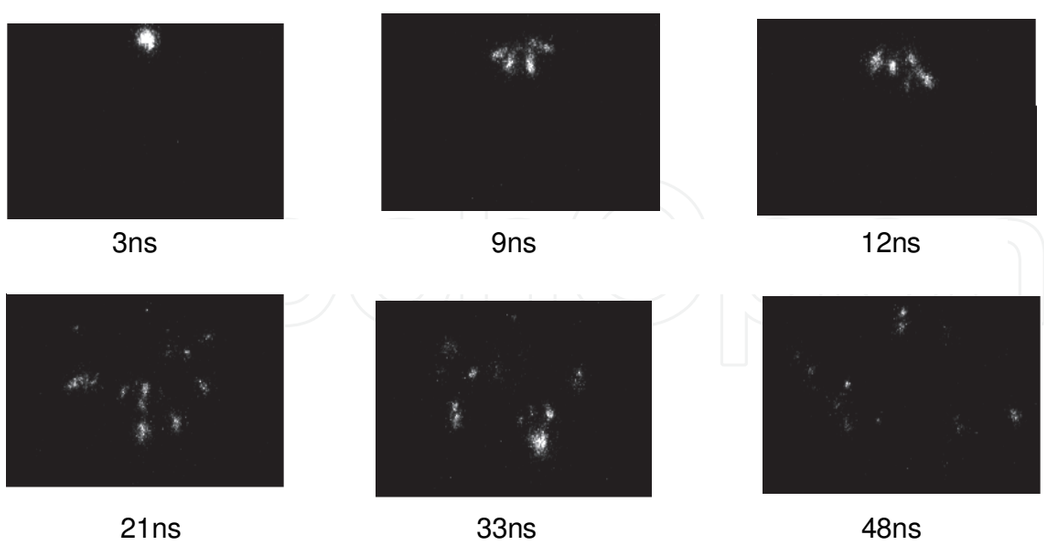

Fig. 8. Time resolved corona discharge pictures at different instants for dry air at atmospheric pressure: Maximum voltage magnitude=8kV, pulse voltage width=40µs, inter-electrode distance=8mm and pin radius=25µm, exposure time = 3ns, reference intensity image=21ns

To summarize, the voltage pulsed corona micro-discharges are characterized by a streamer branching structure and the propagation of multiple primary and secondary streamers.
Relations between pulsed and DC voltage conditions can be pointed out using a large width voltage pulse. In this case, several micro-discharges are able to cross the inter-electrode gap during a single voltage pulse. Fig. 9 shows the morphology of the first the 18 corona micro-discharges generated between a pin and a plane using a high voltage pulse of 20ms of duration.

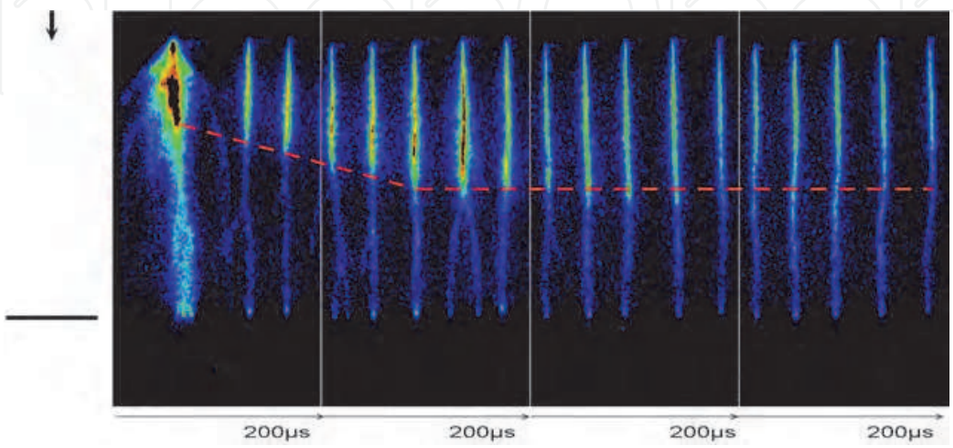

Fig. 9. Streak pictures of the successive corona micro-discharges induced in dry air by a pulse voltage of 20 ms duration and 7.2 kV magnitude (Abahazem et al. 2008).

The branching phenomenon is clearly observed in the first corona micro-discharge with the simultaneous development of a high number of filaments (see the first corona micro-discharge in Fig. 9). Then, during about 400µs, the following discharges present a trunk expansion (shown by the red line in Fig. 9) in front of which a low number of filaments develop. A complete mono-filament structure appears after tens of discharges. Their characteristics are the same as those observed under DC high voltage condition. Thus, the more luminous trails in the discharge pictures of Fig. 9 correspond in fact to the development of the secondary streamers which extend gradually from the point towards the plane. Therefore, the formation of the mono-filament structure can be explained as a result of complex thermal and kinetics memory effects induced in the secondary streamer between each successive discharge.

2.4 Induced neutral gas perturbations

Even if micro-discharges are non thermal plasmas, their propagation can affect the neutral background gas (Eichwald et al. 1997, Ono & Oda b, 2004, Batina et al, 2002). In all cases, the micro-discharges modify the chemical composition of the medium (Kossyi et al. 1992, Eichwald et al. 2002, Dorai & Kushner 2003). In fact, the streamer heads propagate high energetic electrons that create radicals, dissociated, excited and ionized species by collision with the main molecule of the gas. Indeed, we have to keep in mind the low proportion of electrons and more generally of charged particles present in non-thermal plasma. At atmospheric pressure, and in the case of corona micro-discharge, we have about one million of neutral particles surrounding every charged species. Therefore, the collisions charged-neutral particles are predominant. During the discharge phase (which is associated to the

current pulse), the radical and excited species are created inside the micro-discharge volume. But during the post-discharge phase (i.e. between two successive current pulses) these active species react with the other molecules and atoms and diffuse in the whole reactor volume. If a gas flow exists, they are also transported by the convective phenomena. However, convective transport can also be induced by the micro-discharges themselves. Indeed, the momentum transfers between heavy charged particles and background gas are able to induce the so called "electric wind". The random elastic collisions between charged and neutral particles directly increase the gas thermal energy. Furthermore, the inelastic processes modify the internal energy of some molecules thus leading to rotational, vibrational and electronic excitations, ionisation and also dissociation of molecular gases. After a certain time, the major part of these internal energy components relaxes into random thermal energy. However, during the lifetime of micro-discharges (some hundred of nanoseconds), only a fraction of this energy, which in fact corresponds mainly to the rotational energy and electronic energy of the radiative excited states, relaxes into thermal form. The other fraction of that energy, which is essentially energy of vibrational excitation, relaxes more slowly (after 10^{-5}s up to 10^{-4}s). The thermal shock during the discharge phase can induce pressure waves and a diminution of the gas density and the vibrational energy relaxation can increase the mean gas temperature (Eichwald et al. 1997). All these complex phenomena induce memory effects between each successive micro-discharge. In fact, the modification of the chemical composition of the gas can favour stepwise ionisation with the pre-excited molecule (like metastable and vibrational excited species), the gas density modification influences all the discharge parameters which are function of the reduced electric field E/N (E being the total electric field and N the background gas density) and the three body reaction that are also function of the gas density. Furthermore, the local temperature increase also modifies the gas reactivity because the efficiency of some reactions depends on the gas temperature following Arrhenius law. Therefore, the complete simulation of micro-discharges has to take into account all these complex phenomena of discharge and gas dynamics.

2.5 The complete micro-discharge model in the hydrodynamics approximation

The complete simulation of the discharge reactor, in complement to experimental studies can lead to a better understanding of the physico-chemical activity triggered during micro-discharge development and relaxation. Nowadays, in order to take into account the complex energetic, hydrodynamics and chemical phenomena that can influence the corona plasma process, the full simulation of the non thermal plasma reactor can be undertaken by coupling the following models:

- The external electric circuit model,
- the electro-hydrodynamics model,
- the background gas hydrodynamics model including the vibrational excited state evolution,
- the chemical kinetics model,
- and the basic data model which gives the input data for the whole previous models.

Each model gives specific information to the others. For example, the electro-hydrodynamics model gives the morphology of the micro-discharge, the electron density and energy as well as the energy dissipated in the ionized channel by the main charged-neutral elastic and inelastic collision processes. This information is coupled with the external

electric circuit model to calculate the micro-discharge impedance needed to follow the inter-electrode voltage evolution. On the other hand, the calculated dissipated energy and momentum transfer are included as source terms in the background gas model in order to simulate the induced hydrodynamics phenomena like electric wind, pressure wave propagation, neutral gas temperature increase, etc. The neutral gas hydrodynamics influences both the discharge dynamics and the chemical kinetics results. For example, the charged transport coefficients depend on the neutral gas density and some main chemical reactions involving neutral species (like the three body reactions) are very dependant on both the gas temperature and density. Finally, the basic data models (Yousfi & Benabdessadok, 1996, Bekstein et al. 2008, Yousfi et al. 1998, Nelson et al. 2003) give the necessary parameters (such as the convective and diffusive charged and neutral transport coefficients, the charged-neutral and neutral-neutral chemical reaction coefficients, the fraction of the energy transferred to the gas from the elastic and inelastic processes, among others) needed to close the total equation systems.

The electro-hydrodynamics model is an approximation of a more rigorous model. The kinetic description based on Boltzmann equations for the charged particles is probably the more rigorous theoretical approach. However the main drawback of the kinetics approach is linked to the treatment of the high number of electrons coming from ionization processes which involves huge computation times especially at atmospheric pressure. Therefore, the classical mathematical model used for solving the micro-discharge dynamics is the macroscopic fluid one also called the hydrodynamics electric model. Up to now, the most commonly used fluid model is the hydrodynamics first order model which involves the first two moments of Boltzmann equation (i.e the density and the momentum transfer conservation equation) for each charged specie coupled with Poisson equation for the space charged electric field calculation (Eichwald et al. 1996). In all cases, the momentum equation can be simplified into the classical drift-diffusion approximation. The obtained system of hydrodynamics equations is then closed by the local electric field approximation which assumes that the transport and reaction coefficients of charged particles depend only on the local reduced electric field E/N. The hydrodynamics approximation is valid as long as the relaxation time for achieving a steady state electron energy distribution function is short compared to the characteristic time of the discharge development. At atmospheric pressure and because of the high number of collisions, the momentum and energy equilibrium times are generally small compared to any macroscopic scale variations of the system. In the hydrodynamics approximation, the coupled set of equations that govern the micro-discharge evolution is the following:

$$\frac{\partial n_c}{\partial t} + \vec{\nabla}.n_c\vec{v}_c = S_c \qquad \forall c \tag{1}$$

$$n_c\vec{v}_c = \mu_c\vec{E} - \overrightarrow{\overrightarrow{D}}_c.\vec{\nabla}n_c \qquad \forall c \tag{2}$$

$$\varepsilon_0 \Delta V = -\sum_c q_c n_c \tag{3}$$

$$\vec{E} = -\vec{\nabla}V \tag{4}$$

These first four equations allow to simulate the behaviour of each charge particle "c" in the micro-discharge (like for example e, N_2^+, O_2^+, O_4^+, O^-, O_2^-, among others). n_c , $\vec{v}_c$, S_c , μ_c , $\vec{\vec{D}}_c$, q_c are respectively the density, the velocity, the source term, the mobility, the diffusive tensor and the charge of each charge specie "c" involved in the micro-discharge. V and $\vec{E}$ are the potential and the total electric field. The source terms S_c represent for each charge specie the chemical processes (like ionization, recombination, attachment, dissociative attachment, among others) as well as the secondary emission processes (like photo-ionisation and photo-emission from the walls (Kulikovsky, 2000, Hallac et al. 2003, Segur et al. 2006)). The transport equations of charged particles are not only strongly coupled through the plasma reactivity but also through the potential and electric field equations. Indeed, in equation (3) the potential and therefore the electric field in equation (4) are directly dependant on the variation of the density of the charged species, obtained from solution of equations (1)-(2) requiring the knowledge of transport and reaction coefficients that in turn have a direct dependence on the local reduced electric field E/N. Therefore the simulation of micro-discharge dynamics needs fast and accurate numerical solver to calculate the electric field at each time step (especially in regions with high field gradients like near the streamer head and the electrode pin) and also to propagate high density shock wave.

Even if the solution of the first order hydrodynamics model allows a better understanding of the complex phenomena that govern the dynamics of charged particles in micro-discharges, the experimental investigations clearly show that the micro-discharges have an influence on the gas dynamics that can in turn modify the micro-discharge characteristics. It is therefore necessary to couple the electro-hydrodynamics model with the classical Navier-Stockes equations of a compressible and reactive background neutral gas coupled with the conservation equation of excited vibrational energy (Byron et al. 1960, Eichwald et al. 1997).

$$\frac{\partial \rho m_i}{\partial t} + \vec{\nabla}.\rho m_i \vec{v} + \vec{\nabla}.\vec{J}_i = S_i + S_{ic} \qquad \forall i \tag{5}$$

$$\frac{\partial \rho}{\partial t} + \vec{\nabla}.\rho\vec{v} = 0 \tag{6}$$

$$\frac{\partial \rho \vec{v}}{\partial t} + \vec{\nabla}.\rho\vec{v}\vec{v} = -\vec{\nabla}P - \vec{\nabla}.\vec{\vec{\tau}} + \vec{S}_{qm} \tag{7}$$

$$\frac{\partial \rho h}{\partial t} + \vec{\nabla}.\rho h\vec{v} = \vec{\nabla}.(k\vec{\nabla}T) + \frac{\partial P}{\partial t} + \vec{v}.\vec{\nabla}P + \vec{\vec{\tau}} : \vec{\nabla}\vec{v} - \vec{\nabla}.\sum_i \vec{J}_i h_i + S_h + \frac{\varepsilon_v}{\tau_v} \tag{8}$$

$$\frac{\partial \varepsilon_v}{\partial t} + \vec{\nabla}.\varepsilon_v\vec{v} = S_v - \frac{\varepsilon_v}{\tau_v} \tag{9}$$

The set of equations (5) to (9) are used to simulate the neutral gas behavior and to follow each neutral chemical species "i" (like N, O, O_3, NO_2, NO, N_2 ($A^3\sum_u^+$), N_2 ($a'^1\sum_u^-$), O_2 ($a^1\Delta g$), among others) that are created during the micro-discharge phase. In equations (5) to (9), ρ is the mass density of the background neutral gas, $\vec{v}$ the gas velocity, P the static pressure and

$\overrightarrow{\tau}$ the stress tensor. For each chemical species "i", m_i is the mass fraction, $\vec{J}_i$ the diffusive flux due to concentration and thermal gradients, S_i the net rate of production per unit volume (due to chemical reactions between neutral species) and S_{ic} simulates the creation of new neutral active species during the discharge phase by electron or ion impacts with the main molecules of the gas. h is the static enthalpy, T the temperature, k the thermal conductivity and ε_v the vibrational energy. S_h and S_v are the fraction of the total electron power $\vec{j}.\vec{E}$ transferred during the discharge phase into thermal and vibrational energy. It is generally assumed that the translational, rotational and electronic excitation energies relax quasi immediately into thermal form and that the vibrational energy stored during the discharge phases relaxes after a mean delay time τ_v of some tens of micro-seconds. $\vec{S}_{qm}$ is the total momentum transferred from charged particles to the neutral ones. As already explained, all the discharge parameters (S_c, μ_c, $\overrightarrow{D}_c$, S_{ic}, $\vec{S}_{qm}$, S_h and S_v) are strongly dependent on the reduced electric field (E/N). Therefore the coupling of all the set of equations (1) to (9) for each charged and neutral chemical species will considerably enhance the complexity of the global hydrodynamics model. In fact, each gas density variation can directly affect the development of micro-discharges through the reduced electric field variation.

Finally, the modelling of complex phenomena occurring inside non-thermal reactor filled with complex gas mixtures needs the knowledge of the electron, the ion and the neutral transport and reaction coefficients. The charged and neutral particles kinetics model is therefore one of the method in complement to the experimental one that can be used to calculate or complete the set of basic data. Concerning the charged particles, the more appropriate method to obtain the unknown swarm data is to use a microscopic approach (e.g. a Boltzmann's equation solution for the electron data and a Monte Carlo simulation for the ion data) based on collision cross sections (Yousfi & Benabdessadok, 1996, Bekstein et al. 2008, Yousfi et al. 1998, Nelson et al. 2003). On the other hand the most commonly used method to calculate the neutral swarm data in a gas mixture is the use of the classical kinetic theory of neutral gas mixture (Hirschfielder et al. 1954). The macroscopic charged particles swarm data are given over a large range of either the reduced electric field or the mean electron energy. The whole set of data includes:

- The macroscopic transport coefficients like mobility, longitudinal and transversal diffusion coefficients,
- the reaction coefficients like ionization, attachment, dissociation, radiative or metastable electronic excitation coefficients,
- the mean electron energy exchange frequencies of the elastic, inelastic and super-elastic processes,
- and the mean electron momentum exchange frequency (if the classical drift diffusion approximation is not assumed valid)

The calculation of the scalar (e.g. ionization or attachment frequencies), vectorial (drift velocity), and tensorial (diffusion coefficients) hydrodynamics electron and ion swarm parameters in a gas mixture, needs the knowledge of the elastic and inelastic electron-molecule and ion-molecule set of cross sections for each pure gas composing the mixture. Each collision cross section set involves the most important collision processes that either

affect the charged species transport coefficients or are needed to follow the charged species chemical kinetics and energy or momentum exchange. For example, in order to calculate the macroscopic electron swarm parameters in water vapor, 21 collision cross sections must be known involving the rotational, the vibrational and the electronic excitation processes as well as the ionization, the dissociative attachment and the superelastic processes.
One of the main difficulties is to validate for each pure gas that compose the mixture the chosen set of cross sections. To do that, a first reliable set of electron-molecule and ion-molecule cross section for each individual neutral molecule in the gas mixture must be known. Then, in order to obtain the complete and coherent set of cross sections, it is necessary to adjust this first set of cross sections so as to fit experimental macroscopic coefficients with the calculated ones estimated from either a Boltzmann's equation solution or a Monte Carlo simulation. The obtained solution is certainly not unique but as the comparisons concern several kinds of swarm macroscopic parameters having different dependencies on cross sections (ionization or attachment coefficient, drift velocity, transverse or longitudinal diffusion coefficient) over a wide range of reduced electric field or mean electron energy, most of the incoherent solutions are rejected. Finally, when the sets of cross section are selected for each pure gas, they can be used to calculate with a Bolzmann's equation solution or a Monte Carlo simulation the macroscopic charged species transport and reaction parameters whatever the proportion of the pure gas in the background gas mixture.

2.6 Summary

Micro-discharges are characterized by the development of primary and secondary streamers. As a function of the high voltage applied on the small curvature electrode (DC or pulse), the micro-discharges show either a mono-filament or a large branching structure. The passage from multi-filaments to mono-filament structure can be observed if a sufficiently large high voltage pulse is applied. The transition can be explained through the memory effects accumulated during the previous discharge. The primary streamers propagate fast ionization waves characterized by streamer heads in which the electric field is high enough to generate high energetic electrons like in an electron gun. The streamer head propagates a high charge quantity toward the inter-electrode gap. The micro-plasmas are generated behind the streamer heads. They are small conductive channels that connect the streamer head to the electrode stressed by the high voltage. The primary streamers are then followed by a secondary streamer which is characterized by an electric field extension that ensures the transition between the displacement current and the conductive one when the primary streamer arrives on the cathode. Both primary and secondary streamers create radicals and excited species by electron-molecule impacts. The elastic and inelastic energy transfers generate a chemical activity, a thermal energy increase of the gas and a neutral gas dynamics. To better understand all these complex phenomena, a hydrodynamics model can be used based on conservation equations of charged and neutral particles coupled to Poisson equation for the electric field calculation.

3. Chemical and hydrodynamics activation of gases using corona micro-discharge

3.1 Introduction

During the past two decades several studies have shown that non-thermal plasmas reactor working in ambient air are very efficient sources of active species like charged particles,

radicals and excited species. In fact, and as already explained in the previous sections, in the non-thermal plasma reactor, the majority of the injected electrical energy goes into the generation of energetic electrons, rather than into gas heating. The energy in the micro-plasma is thus directed preferentially to electron-impact dissociation, excitation and ionization of the background gas to generate active species that, in turn, induce the chemical activation of the medium. As a consequence, the non-thermal plasma reactors at atmospheric pressure are used in many applications such as flue gas pollution control (Fridman et al., 2005, Urashima et Chang, 2010), ozone production (Ono & Oda b, 2004), surface decontamination (Clement et al., 2001, Foest et al., 2005) and biomedical field (Laroussi, 2002, Villeger et al., 2008, Sarrette et al., 2010). For many applications, particularly in the removal of air pollutants, decontamination or medicine field, the non-thermal plasma approach would be most appropriate because of its energy selectivity and its capability for simultaneous treatment of pollutants, bacteria or cells for example.

In micro-discharges the active species are created by energetic electrons during the primary and the secondary streamer propagation that last some hundred of nanoseconds. Despite these very fast phenomena, the energy transferred to the gas can initiate shock waves starting from the stressed high voltage electrodes. Furthermore, a part of the electronic energy is stored in the vibrational energy that relaxes in thermal form after some tens of microseconds. Anyway, it is worth to notice, that all the initial energy (chemical, thermal, among others) is transferred inside a very thin discharge filament i.e. in a very small volume compared with the volume of the plasma reactor. Therefore, the efficiency of the processes is correlated to the radical production efficiency during the discharge phase, the number of micro-discharges that cross the inter-electrode gap, the repetition frequency of the discharge and how the radicals are diffused and transported from the micro-discharge towards the whole reactor volume.

In the following sections, the discharge and the post-discharge phase are simulated using the hydrodynamics models presented in section 2.5 in the case of a DC positive pin-to-plan corona reactor in dry air at atmospheric pressure.

3.2 Discharge phase simulation

The simulation conditions are described in detail in reference (Eichwald et al. 2008) as well as the used numerical methods and boundary conditions. To summarize, a DC high voltage of 7.2kV is applied on the pin of a pin-to-plane reactor filled with dry air at atmospheric pressure. The inter-electrode gap is of 7mm, the pin radius is equal to 25μm and photo-ionisation phenomenon is taken into account in the simulation. Results in Fig. 10 and 11 are obtained by coupling equations (1) to (4) for electrons, two negative ions (O^- and O_2^-), four positive ions (N_2^+, O_2^+, N^+ and O^+) and two radical atoms (O, N) reacting following 10 selected reactions. Because of the time scale of the discharge phase (some hundred of nanoseconds), the radical atoms and the main neutral molecules (N_2 and O_2) are supposed to remain static during the discharge phase simulation. Fig. 10 shows the reduced electric field (E/N) expressed in Td ($1Td=10^{-21}$ Vm^2 so that 500Td at atmospheric pressure is equivalent to an electric field of $12MVm^{-1}$). When the high voltage is applied to the pin, some seed electrons are accelerated in the high geometric electric field around the pin. A luminous spot is observed experimentally near the pin thus indicating the formation of excited species due to a high electronic energy. On can notice that the electrons move towards the pin. Furthermore, the electrons gain sufficient energy to perform electronic

avalanches and a plasma spot is created just around the pin. The plasma is a quasi neutral electric gas in which the quantity of negative and positive species is quasi similar. Nevertheless, as the mobility of electrons is much higher than those of positive ions, the electric neutrality of the initial plasma spot is perturbed just in front of the pin. Indeed, the electrons are absorbed by the positive anodic pin while the positive ions remain quasi static due to their mass inertia. A positive charged space is formed and the electric field is no more at his maximum on the pin but just in front of it. This situation can be seen at time t=20ns in the first picture of Fig. 10.

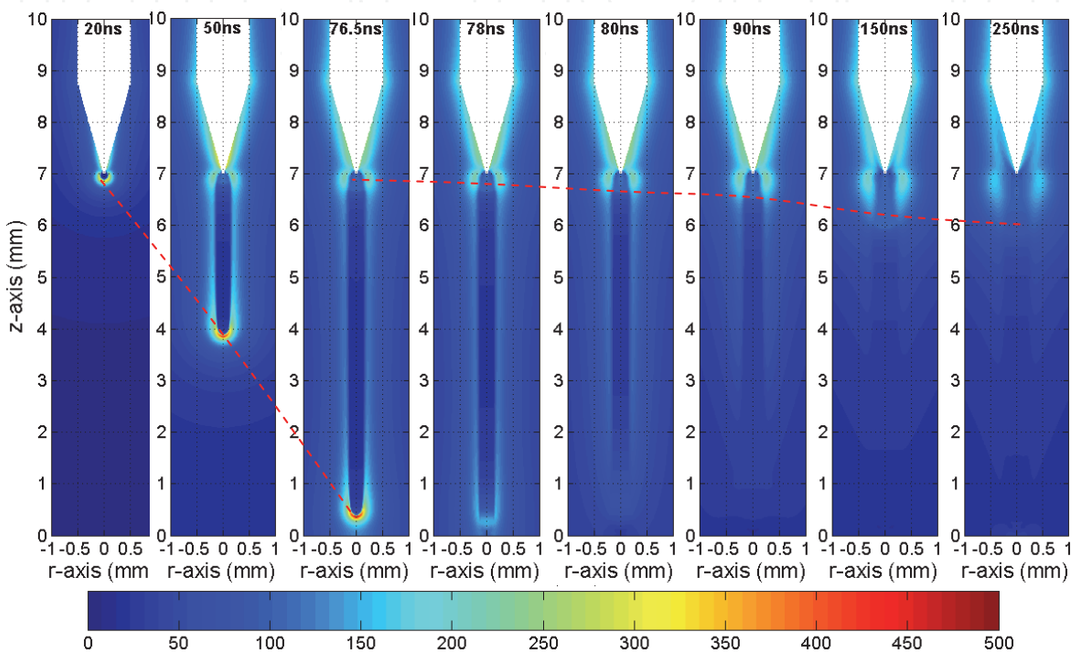

Fig. 10. Reduced electric field profile (500Td=12MVm^{-1}) in function of time

A streamer head is created that propagates from the pin towards the plane. This streamer head can be interpreted as the propagation of a positive charge space shock wave. At each time of its propagation, new seed electrons are created in front of the streamer head by photo-ionisation processes. These electrons are accelerated in the high electric field and their energy is high enough to ionize, dissociate and excite the main molecules of the gas. When the electrons have crossed the streamer head they drift towards the pin inside a small conductive plasma channel that connects the streamer head to the pin. A micro-plasma is formed behind the streamer head and is constricted by a cylinder of space charged electric field. A quasi-homogeneous small value of electric field is maintained inside the micro-plasma in order to allow the drift of electrons from the streamer head to the pin that ensures the continuity of the total current density. The time laps needed for the streamer head to cross the inter-electrode gap is associated with the primary streamer propagation of the micro-discharge phase. The streamer head propagates a charge quantity which is absorbed by the cathode plane as soon as it arrives on the cathode plane. It results to the first current peak observed in Fig. 4 for a high voltage DC condition. The first red dashed curve in Fig. 10 follows the trail left by the high electric field of the streamer head. Its shape corresponds to the luminous trail observed by streak camera shown in Fig. 3. When the primary streamer

arrives at the cathode plane, a secondary streamer starts its propagation from the pin. The secondary streamer is an electric field plateau extension of value of about 100Td. This extension ensures the continuity of the total current when the total charge space transported by the streamer head is absorbed at the cathode (Eichwald et al. 2008, Bastien & Marode, 1985). The second red dashed curve follows the plateau extension. The evolution of the luminous trail left by the secondary streamer shown in Fig. 3 is due to the excited species created by the energetic electrons inside the secondary streamer expansion. Fig. 11 shows the radical O density after 150ns. The simulation indicates that about 70% of the radical O is produced inside the secondary streamer by dissociative collisions between electrons and O_2 molecules in reaction $e+O_2 \rightarrow O + O$. The concentration of O radical is also high near the cathode plane due to a higher electric field magnitude inside the streamer head when it reaches the cathode.

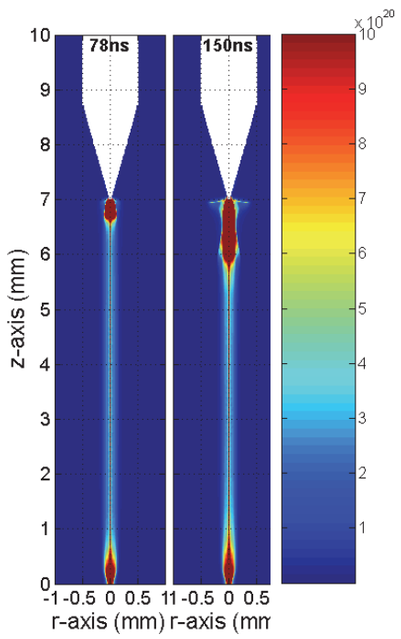

Fig. 11. O radical profile (m^{-3})

The effect on the neutral gas dynamics induced by the micro-discharge propagation is shown in Fig. 12 and 13. Fig. 12 shows the temperature profile of the background neutral gas at 0.1µs (=100ns) and 0.3µs (=300ns). Fig. 13 shows the pressure profile from 0.1µs to 4µs. The gas temperature just on the pin reaches some thousands of Kelvin but a mean value of about 700°K is obtained around the point. This value is coherent with experimental results obtained under very similar condition (Spyrou et al., 1992). The thermal shock creates high pressure gradients (see Fig. 13 at 0.1µs) and induces the gas expansion (see Fig. 13). Due to the inertia principle, the mass density near the point decreases more gradually in a time scale greater than the temperature increase. The gas expansion is characterised by a cylindrical and a spherical shock wave (see Fig. 13 from 0.3 to 0.9µs). Indeed, the initial pressure gradients (which induced the gas motion) follow the temperature ones which are constricted along the axis and inside the micro-plasma channel. We therefore observe a cylindrical pressure wave (represented by two vertical lines in the flat pressure mappings of Fig. 13) that propagates from the streamer axis towards the whole domain. The complex

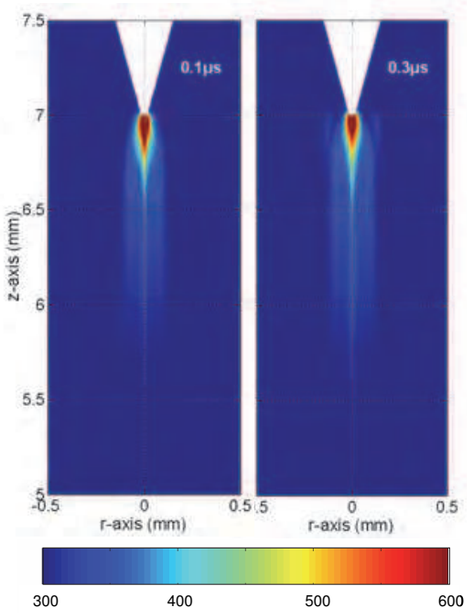

Fig. 12. Gas temperature (°K) profile near the point

structure of the pressure gradients near the point induces a spherical pressure wave superimposed to the cylindrical one. Such kind of spherical pressure waves were already observed experimentally (Ono & Oda b, 2004) using the laser Schlieren method. Furthermore, the simulation shows that the spherical shock wave propagates at the speed of sound as in the case of experimental work (Ono & Oda b, 2004).

In this kind of simulation the effects of temperature and gas density variations on the streamer development are not taken into account. However, it should be in further works because if the gas density varies it will modify the reduced electric flied (E/N) and therefore the behaviour of the charged particles whose properties (like mobility, ionisation frequency,…) completely depend on the reduced electric field. Nevertheless, the previous results are able to give the initial profiles of all the source terms needed to simulate the post-discharge phase evolution.

3.3 Post-discharge phase simulation

The discharge phase simulation gives very clear information on the gas dynamics and the spatio-temporal evolution of each active species of the background gas mixture. However, the time and space scales between the discharge phase and the post-discharge phase are completely different. Indeed, the micro-discharge generated micro-plasma in some hundred of nanoseconds while post-discharge phase must be considered with centimetre scale and milliseconds time laps. A complete simulation of both coupled phenomena for multi-pin reactor needs therefore adaptive meshes from micrometer to centimetre scale and also adaptive time scale from picoseconds (in order to follow the nano-scale discharge phenomena) up to fraction of milliseconds. This means a large number of discrete spatial cells and a huge computing time. In order to overcome these difficulties, on can assume that the effects of the discharges on the background gas can be simulated by locally injected inside the micro-discharge volumes and only during the discharge phase, average source terms estimated from the complete discharge phase model.

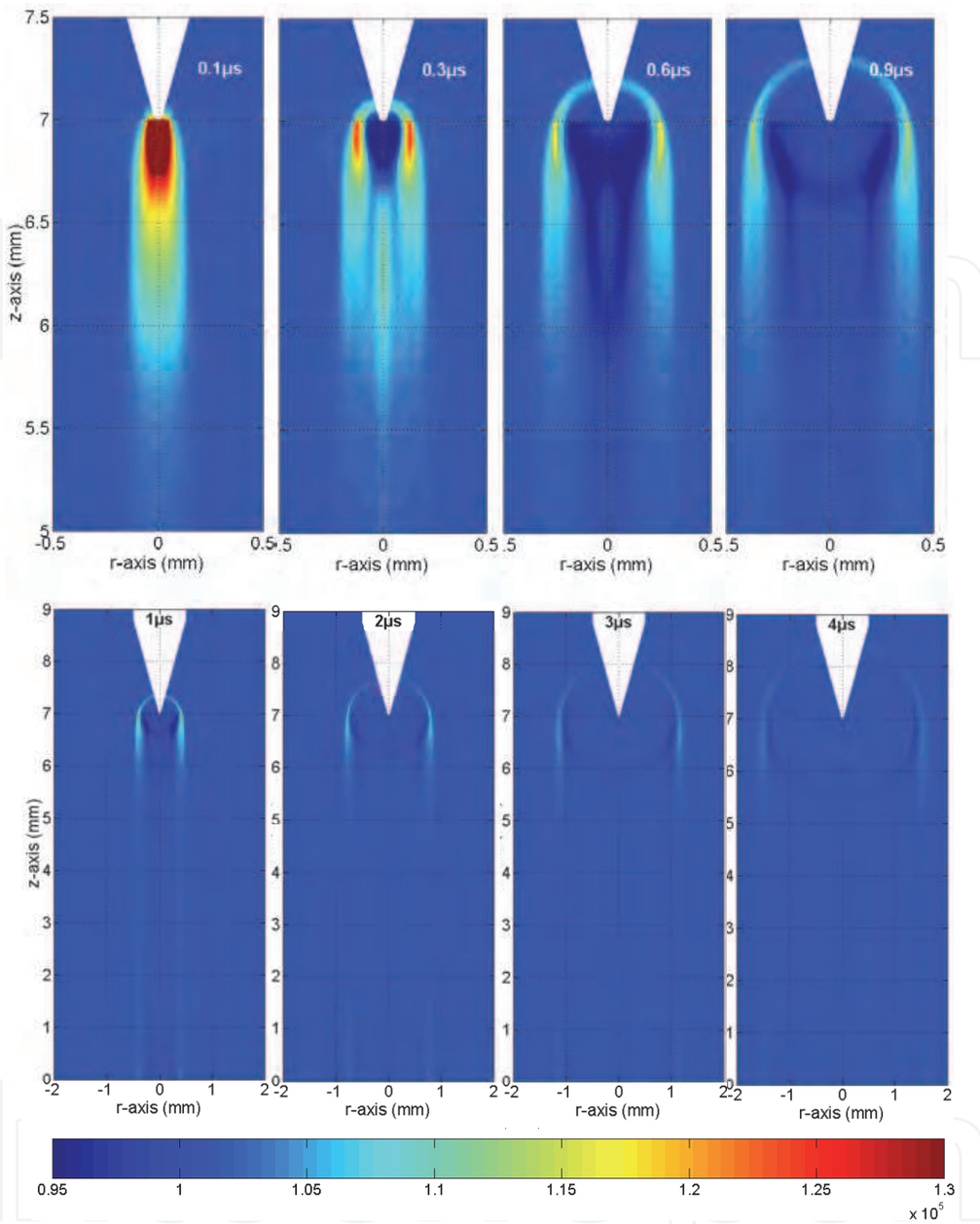

Fig. 13. Pressure wave (Pa) near the point (from 0.1 to 0.9µs) and in the whole domain (from 1 to 4µs)

As an example, let us suppose the multi-pin reactor described in Fig. 14. The domain is divided with square structured meshes of 50µm×50µm size. A DC high voltage of 7.2kV is applied on the pins. During each discharge phase, monofilament micro-discharges are created between each pin and the plane with a natural frequency of 10kHz. The micro-discharges have an effective diameter of 50µm which correspond to the size of the chosen cells. Therefore, it is possible to inject in the cells located between each pin and the plane specific profiles of active source species and energy that will correspond the micro-discharge effects.

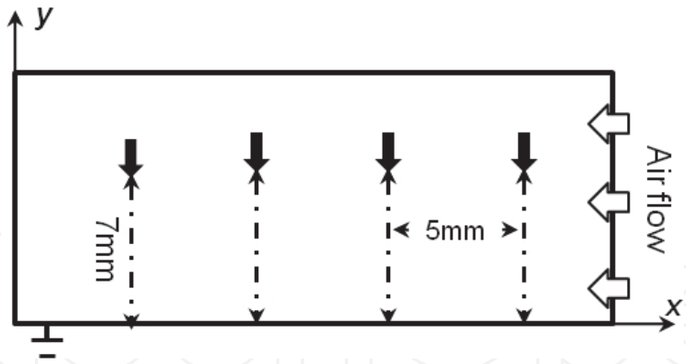

Fig. 14. 2D Cartesian simulation domain of the multi-pin to plane corona discharge reactor.

As an example, consider equation (5) of section 2.5 applied to O radical atoms ('i"=O).

$$\frac{\partial \rho m_O}{\partial t} + \vec{\nabla}.\rho m_O \vec{v} + \vec{\nabla}.\vec{J}_O = S_O + S_{Oc}$$

The challenge is to correctly estimate the source term S_{Oc} inside the volume of each micro-discharge. As the radial extension of the micro-discharges is equal to the cell size, the source term between each pin and the plane depends only on variable z. The average source term responsible of the creation of O radical during the discharge phase is therefore expressed as follow:

$$S_{Oc}(z) = \frac{1}{r_d}\frac{1}{t_d}\int_0^{r_d}\int_0^{t_d} s_{Oc}(t,r,z)\,dtdr \tag{10}$$

t_d is the effective micro-discharge duration, r_d the effective micro-discharge radius and $s_{Oc}(t,r,z)$ the source terms ($m^{-3}s^{-1}$) of radical production during the discharge phase (i.e. $k(E/N)n_e n_{O2}$ for reaction $e + O_2 \rightarrow O + O$ where k(E/N) is the corresponding reaction coefficient). All the data in equation (10) come from the complete simulation of the discharge phase. In the present simulation conditions, specific source terms are calculated for 5 actives species that are created during the discharge phase ($N_2(A^3\sum u^+)$, $N_2(a'^1\sum u^-)$, $O_2(a^1\Delta g)$, N and O).

The energy source terms in equations (8) and (9) are estimated using equations (11) and (12):

$$S_h(z) = \rho C_p \frac{1}{r_d}\frac{1}{t_p^2}\int_0^{r_d}\int_0^{t_p} T(t_p,r,z)\,dtdr \tag{11}$$

$$S_v(z) = \frac{1}{r_d}\frac{1}{t_d}\int_0^{r_d}\int_0^{t_d} f_v \vec{J}.\vec{E}\,dtdr \tag{12}$$

In equation (12), $\vec{j}.\vec{E}$ is the total electron density power gained during the discharge phase and f_v the fraction of this power transferred into vibrational excitation state of background gas molecules. One can notice the specificity of equation (11) related with the estimation of the direct random energy activation of the gas. In this equation, t_p is the time scale of the pressure wave generation rather than the micro-discharge duration t_d. In fact, during the

post-discharge phase, the size of discrete cells is not sufficiently small to follow the gradients of pressure wave generated by thermal shock near the point (see Fig. 13). However, pressure waves transport a part of the stored thermal energy accumulated around each pin. From 0.1µs to 0.3µs, the gas temperature on the pins decreases from about 3000°K down to about 1200°K. After this time, the temperature variation in the micro-discharge volume is less affected by the gas dynamics. The diffusive phenomena become predominant. Therefore, taken into account the mean energy source term at time t_d will overestimate the temperature enhancement on the pins during the post-discharge phase simulation. As a consequence, the time t_p is chosen equal to 300ns i.e. after the pressure waves have left the micro-discharge volume.

As an example, Fig. 15 shows the temperature profile obtained at $t=t_p$ just after the first discharge phase. The results were obtained using the Fluent Sofware in the simulation conditions described in Fig. 14. As expected and just after the first discharge phase, the enhancement of the gas temperature is confined only inside the micro-plasma filaments located between each pin and the plane. The temperature profile along the inter-electrode gap is very similar to the one obtained by the complete discharge phase simulation (see Fig. 12). It is also the case for the active source terms species. Fig. 16 shows at time $t=t_d$, the axial profile of some active species that are created during the discharge phase. The curves of the discharge model represent the axial profile density averaged along the radial direction. In

Fig. 15. Gas temperature profile after the first discharge phase at $t=t_p$ = 300ns.

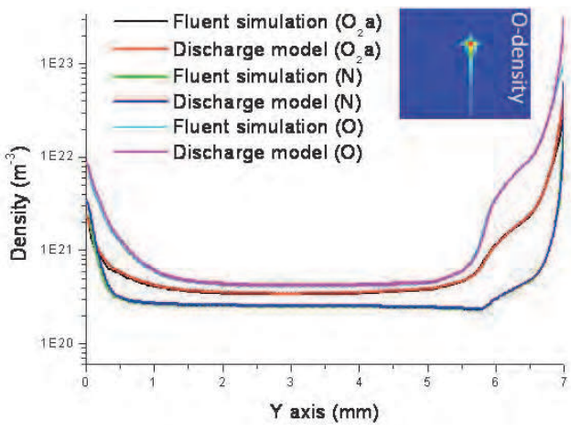

Fig. 16. Comparison of numerical solutions given by the completed discharge and Fluent models at t_d=150 ns for O, N and O_2 ($a^1\Delta g$) densities. The zoom box shows, as an example, the O radical profile near a pin.

the case of the O radical, the density profile of Fig. 11 was averaged along the radial direction until r_d=50µm and drawn in Fig. 16 with the magenta color. The light blue color curve represents the O radical profile obtained with the Fluent Software when the specific source term profile $S_{Oc}(z)$ is injected between a pin and the cathode plane in the simulation conditions of Fig. 14.

In the following results, the complete simulation of the successive discharge and post-discharge phases involves 10 neutral chemical species (N, O, O_3, NO_2, NO, O_2, N_2, N_2 ($A^3\sum_u^+$), N_2 ($a'^1\sum_u^-$) and O_2 ($a^1\Delta g$)) reacting following 24 selected chemical reactions. The pin electrodes are stressed by a DC high voltage of 7.2kV. Under these experimental conditions the current pulses appear each 0.1ms (i.e. with a repetition frequency of 10KHz). It means that the previous described source terms are injected every 0.1ms during laps time t_d or t_p and only locally inside the micro-plasma filament located between each pin and the plane. The lateral air flow is fixed with a neutral gas velocity of 5m.s^{-1}.

Pictures in Fig. 17 show the cartography of the temperature and of the ozone density after 1ms (i.e. after 10 discharge and post-discharge phases). One, two, three or four pins are stressed by the DC high voltage. Pictures (a) show that for the mono pin case, the lateral air flow and the memory effect of the previous ten discharges lead to a wreath shape of the space distribution of both the temperature and the ozone density.

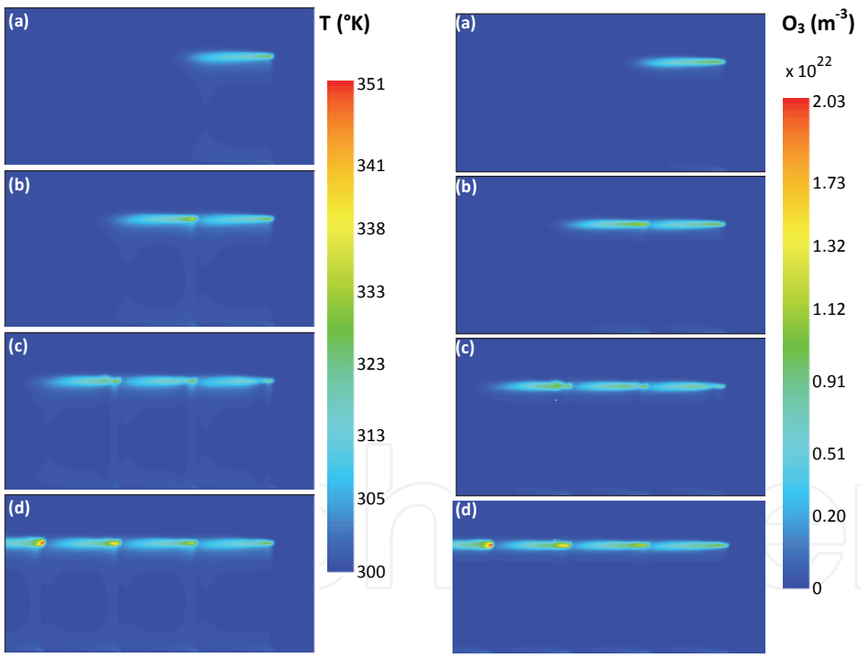

Fig. 17. Temperature and ozone density profile at 1ms i.e. after ten discharge and post-discharge phases. The number of high voltage pin is respectively (a) one, (b) two, (c) three and (d) four. The lateral air flow is 5m.s^{-1}.

The temperature and the ozone maps are very similar. Indeed, both radical and energy source terms are higher near the pin (i.e. inside the secondary streamer area expansion as it was shown in section 3.2). Furthermore, the production of ozone is obviously sensitive to the gas temperature diminution since it is mainly created by the three body reaction $O + O_2 + M \rightarrow O_3 + M$ (having a reaction rate inversely proportional to gas temperature).

For more than one pin, the temperature and ozone wreaths interact each other and their superposition induce locally a rise of both the gas temperature and ozone density (see Fig. 17). The local maximum of temperature is around 325K for one pin case and increases up to 350K for four anodic pins.
The average temperature in the whole computational domain remains quasi constant and the small variations show a linear behavior with the number of anodic pins. The same linear tendency is observed for the ozone production in Fig. 18. After 1ms, and for the four pins case, the mean total density inside the computational domain reaches $4x10^{14}$ cm^{-3}.

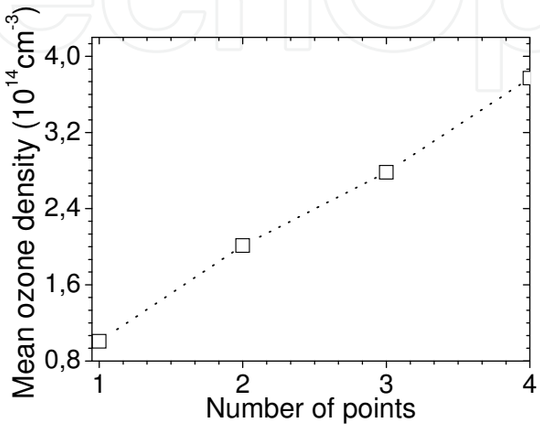

Fig. 18. Mean ozone density increase inside the computational domain of Fig. 14 as a function of the number of pins

3.4 Summary

The complete simulation of all the complex phenomena that are triggered by micro-discharges in atmospheric non thermal plasma was found to be possible not as usually done in the literature only for 0D geometry but also in multidimensional geometry. In DC voltage conditions, a specific first order electro-hydrodynamics model was used to follow the development of the primary and secondary streamers in mono pin-to-plane reactor. The simulation results reproduce qualitatively the experimental observations and are able to give a full description of micro-discharge phases. Further works, already undertaken in small dimensions or during the first instants of the micro-discharge development (Pancheshnyi 2005, Papageorgiou et al. 2011), have to be achieved in 3D simulation in order to describe the complex branching structure for pulsed voltage conditions. Nevertheless, the micro-discharge phase simulation gives specific information about the active species profiles and density magnitude as well as about the energy transferred to the background gas. All these parameters were introduced as initial source terms in a more complete hydrodynamics model of the post-discharge phase. The fist obtained results show the ability of the Fluent software to solve the physico-chemical activity triggered by the micro-discharges.

4. Conclusion

The present chapter was devoted to the description of the hydrodynamics generated by corona micro-discharges at atmospheric pressure. Both experimental and simulation tools have to be exploited in order to better characterise the strongly coupled behaviour of micro-

discharges dynamics and background gas dynamics. The experimental devices have to be very sensitive and precise in order to capture the main characteristics of nanosecond phenomena located in very thin filaments of micro scale extension. However, the recent evolution of experimental devices (ICCD or streak camera, DC and pulsed high voltage supply, among others) allow to better understand the physics of the micro-discharge. Furthermore, recent simulation of the micro-discharges involving the discharge and post-discharge phase in multidimensional dimension was found to give precise information about the chemical and hydrodynamics activation of the background gas in an atmospheric non-thermal plasma reactor. These kinds of simulation results, coupled with experimental investigation, can be used in future works for the development of new design of plasma reactor very well adapted to the studied application either in the environmental field or biomedical one.

5. Acknowledgment

All the simulations were performed using the HPC resources from CALMIP (Grant 2011-[P1053] - www.calmip.cict.fr/spip/spip.php?rubrique90)

6. References

Abahazem, A.; Merbahi, N.; Ducasse, O.; Eichwald, O. & Yousfi, M. (2008), Primary and secondary streamer dynamics in pulsed positive corona discharges, *IEEE Transactions on Plasma Science* , Vol. 36, No. 4, pp. 924-925

Bastien, F. & Marode, E. (1985), Breackdown simulation of electronegative gases in non-uniform field, *Journal of Physics D: Applied Physics*, Vol. 18, pp. 377-393

Batina, J.; Noel, F.; Lachaud, S. ; Peyrous, R. & Loiseau, J. F. (2001) Hydrodynamical simulation of the electric wind in a cylindrical vessel with positive point-to-plane device, *Journal of Physics D: Applied Physics*, Vol. 34, pp. 1510–1524

Bekstein, A.; Benhenni, M.; Yousfi, M.; Ducasse, O. & Eichwald, O. (2008), Ion swarm data of N_4^+ in N_2, O_2 , and dry air for streamer dynamics simulation , *European Physics Journal Applied Physics*, Vol. 42, pp. 33-40

Briels, T. M. P.; Kos J.; van Veldhuizen E. M. & Ebert, U. (2006), Circuit dependence of the diameter of pulsed positive streamers in air, Journal of Physics D: Applied Physics, Vol. 39, pp. 5201–5210

Byron, R.; Stewart, W. E.; Lightfoot E. N. (1960) Transport Phenomena, John Wiley & Sons

Clement, F.; Held, B.; Soulem N. & Spyrou N. (2001). Polystyrene thin films treatment under DC pulsed discharges conditions in nitrogen, *The European Physical Journal, Applied Physics*, Vol. 13, pp. 67-75

Dubois, D.; Merbahi, N.; Eichwald, O.; Yousfi, M.; Ducasse, O. & Benhenni, M. (2007), Electrical analysis of DC positive corona discharge in air and N_2, O_2 and CO_2 mixtures, *Journal of Applied Physics*, Vol. 101, Issue 5, pp. 053304-053304-9

Dorai R. & Kushner M. (2003) Consequences of unburned hydrocarbons on microstreamer dynamics and chemistry during plasma remediation of NO*x* using dielectric barrier discharges *Journal of Physics D: Applied Physics*,. Vol. 36, pp. 1075–1083

Eichwald, O.; Ducasse, O.; Merbahi, N.; Yousfi, M. & Dubois, D. (2006), Effect of order fluid models on flue gas streamer dynamics", *Journal of Physics D: Applied Physics*, Vol. 39, pp. 99–107

Eichwald, O.; Yousfi M.; Hennad A.& Benabdessadok M. D. (1997) Coupling of chemical kinetics, gas dynamics, and charged particle kinetics models for the analysis of NO reduction from flue gases, *Journal of Applied Physics*, Vol. 82, No. 10, pp. 4781-4794

Eichwald, O.; Ducasse, O.; Dubois, D.; Abahazem, A.; Merbahi, N.; Benhenni M. & Yousfi, M. (2008) Experimental analysis and modelling of positive streamer in air: towards an estimation of O and N radical production, J. Phys. D: Appl. Phys., Vol. 41 234002 (11pp)

Eichwald, O., Guntoro, N. A.; Yousfi, M. & Benhenni M. (2002) Chemical kinetics with electrical and gas dynamics modelization for NO*x* removal in an air corona discharge *Journal of Physics D: Applied Physics*, Vol. 35, pp. 439-450

Foest, R.; Kindel, E.; Ohl, A.; Stieber, M. & Weltmann, K. D. (2005) Non-thermal atmospheric pressure discharges for surface modification Plasma Physics Controlled Fusion, Vol. 47, B525–B536

Fridman A.; Chirokov, A. & Gutsol, A. (2005), TOPICAL REVIEW, Non-thermal atmospheric pressure discharges, *Journal of Physics D: Applied Physics*, Vol. 38, R1-R24

Hallac, A.; Georghiou, G. E. & Metaxas, A; C. (2003) Secondary emission effects on streamer branching in transient non-uniform short-gap discharges, *Journal Of Physics D: Applied Physics*, Vol. 36 pp. 2498–2509

Hirschfielder, J. O.; Curtiss, F. E. and Bird R. B. (1954) Molecular theory of gases and liquids, Wiley, New York

Kossyi, I. A. ; Yu Kostinsky, A. ; Matveyev A. A. & Silakov V. P., (1992), Kinetic scheme of the non equilibrium discharge in nitrogen-oxygen mixtures, *Plasma Sources Sciences and Technologies*, Vol.1, pp. 207-220

Kulikovsky, A. A. (2000), The role of photoionisation in positive streamer dynamics, *Journal of Physics D: Applied Physics*, Vol. 33, pp. 1514-1524

Laroussi, M. (2002). Nonthermal decontamination of biological media by atmospheric-pressure plasmas: review, analysis and prospects, *IEEE Transactions on Plas. Science*, Vol. 30, No.4, pp. 1409-1415

Loeb, L. B. (1961) Basic processes of gaseous electronics, University of California Press, Berkeley.

Loeb, L. B. (1965) Electrical coronas, University of California Press, Berkeley.

Marode, E. (1975), The mechanism of spark breakdown in air at atmospheric pressure between a positive point an a plane. I. Experimental: Nature of the streamer track, *Journal of Applied Physics*, Vol. 46, No. 5, pp. 2005-2015

Nelson, D.; Benhenni, M.; Eichwald, O. & Yousfi, M. (2003), Ion swarm data for electrical discharge modeling in air and flue gas, *Journal of Applied Physics*, Vol. 94, pp. 96-103

Ono, R. & Oda, T. a (2004). Spatial distribution of ozone density in pulsed corona discharges observed by two-dimensional laser absorption method, *Journal of Physics D: Applied Physics,* Vol. 37, pp. 730-735.

Ono, R. & Oda, T. b (2004) Visualization of Streamer Channels and Shock Waves Generated by Positive Pulsed Corona Discharge Using Laser Schlieren Method, Japanese Journal of Applied Physics, Vol. 43, No. 1, 2004, pp. 321–327

Pancheshnyi, S. (2005), Role of electronegative gas admixtures in streamer start, propagation and branching phenomena, *Plasma Sources Science and Technology*, Vol. 14, pp. 645–653

Papageorgiou, L., Metaxas, A. C. & Georghiou, G. E. (2011), Three-dimensional numerical modelling of gas discharges at atmospheric pressure incorporating photoionization phenomena, *Journal of Physics D: Applied Physics*, Vol. 44, 045203 (10pp).

Penetrante, B. M. & Schultheis, S. E. (1993), Nonthermal Plasma Techniques for Pollution Control, Part A&B, Editors, NATO ASI Series Vol. G 34, Springer-Verlag, Karlsruhe.

Sarrette, J. P. ; Cousty, S. ; Merbahi, N. ; Nègre-Salvayre, A. & F. Clément (2010), Observation of antibacterial effects obtained at atmospheric and reduced pressures in afterglow conditions, *European Physical Journal. Applied. Physics,* Vol. 49 13108

Segur, P.; Bourdon, A.; Marode, E., Bessieres D. & Paillol J. H. (2006) The use of an improved Eddington; approximation to facilitate the calculation of photoionization in streamer discharges, Plasma Sources Sciences and Technologies, Vol. 15, pp. 648–660

Sigmond, R. S. (1984), The residual streamer channel: Return strockes and secondary streamers, *Journal of Applied Physics*, Vol. 56, No. 5, pp. 1355-1370

Spyrou, N.; Held, B.; Peyrous, R.; Manassis, Ch. & Pignolet, P. (1992) Gas temperature in a secondary streamer discharge: an approach to the electric wind, Journal of Physics D: Applied Physics, Vol. 25, pp. 211-216

van Veldhuizen, E. M. & Rutgers, W. R. (2002), Pulsed positive corona streamer propagation and branching, *Journal of Physics D: Applied Physics*, Vol. 35, pp. 2169–2179

Urashima K. & J. S. Chang (2010) Removal of Volatile Organic Compounds from Air Streams and Industrial Flue Gases by Non-Thermal Plasma Technolog, *IEEE Transactions on Dielectrics and Electrical Insulation,* Vol. 7 No. 5, pp. 602-614

Villeger, S.; Sarrette, J. P.; Rouffet, B. ; Cousty S. & Ricard A. (2008), Treatment of flat and hollow substrates by a pure nitrogen flowing post discharge: Application to bacterial decontamination in low diameter tubes, *European Physical Journal. Applied. Physics*, Vol. 42, pp. 25-32.

Winands, G.; Liu, Z.; Pemen, A.; van Heesch, E.; Yan, K. & van Veldhuizen, E. (2006), Temporal development and chemical efficiency of positive streamers in a large scale wire-plate reactor as a function of voltage waveform parameters, *Journal of Physics D: Applied Physics*, Vol. 39, pp. 3010–3017

Yousfi, M. & Benabdessadok, M. D. (1996), Boltzmann equation analysis of electron-molecule collision cross sections in water vapor and ammonia, *Journal of Applied Physics*, Vol. 80, pp. 6619-6631

Yousfi, M.; Hennad, A. & Eichwald, O. (1998), Improved Monte Carlo method for ion transport in ion-molecule asymmetric systems at high electric fields, *Journal of Applied Physics*, Vol. 84, No. 1, pp. 107-104

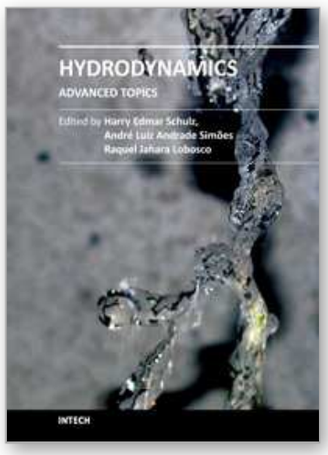

Hydrodynamics - Advanced Topics
Edited by Prof. Harry Schulz

ISBN 978-953-307-596-9
Hard cover, 442 pages
Publisher InTech
Published online 22, December, 2011
Published in print edition December, 2011

The phenomena related to the flow of fluids are generally complex, and difficult to quantify. New approaches - considering points of view still not explored - may introduce useful tools in the study of Hydrodynamics and the related transport phenomena. The details of the flows and the properties of the fluids must be considered on a very small scale perspective. Consequently, new concepts and tools are generated to better describe the fluids and their properties. This volume presents conclusions about advanced topics of calculated and observed flows. It contains eighteen chapters, organized in five sections: 1) Mathematical Models in Fluid Mechanics, 2) Biological Applications and Biohydrodynamics, 3) Detailed Experimental Analyses of Fluids and Flows, 4) Radiation-, Electro-, Magnetohydrodynamics, and Magnetorheology, 5) Special Topics on Simulations and Experimental Data. These chapters present new points of view about methods and tools used in Hydrodynamics.

How to reference
In order to correctly reference this scholarly work, feel free to copy and paste the following:

O. Eichwald, M. Yousfi, O. Ducasse, N. Merbahi, J.P. Sarrette, M. Meziane and M. Benhenni (2011). Electro-Hydrodynamics of Micro-Discharges in Gases at Atmospheric Pressure, Hydrodynamics - Advanced Topics, Prof. Harry Schulz (Ed.), ISBN: 978-953-307-596-9, InTech, Available from: http://www.intechopen.com/books/hydrodynamics-advanced-topics/electro-hydrodynamics-of-micro-discharges-in-gases-at-atmospheric-pressure

INTECH
open science | open minds

InTech Europe
University Campus STeP Ri
Slavka Krautzeka 83/A
51000 Rijeka, Croatia
Phone: +385 (51) 770 447
Fax: +385 (51) 686 166
www.intechopen.com

InTech China
Unit 405, Office Block, Hotel Equatorial Shanghai
No.65, Yan An Road (West), Shanghai, 200040, China
中国上海市延安西路65号上海国际贵都大饭店办公楼405单元
Phone: +86-21-62489820
Fax: +86-21-62489821

IntechOpen